Effect of an electric field on air filament decay at the trail of an intense femtosecond laser pulse

Sergey Bodrov,[1,2,*] Nickolay Aleksandrov,[3] Maxim Tsarev,[1,2] Alexey Murzanev,[1] Igor Kochetov,[4] and Andrey Stepanov[1]

[1]*Institute of Applied Physics, Russian Academy of Sciences, Nizhny Novgorod 603950, Russia*

[2]*University of Nizhny Novgorod, Nizhny Novgorod 603950, Russia*

[3]*Moscow Institute of Physics and Technology, Dolgoprudny 141700, Russia*

[4]*Troitsk Institute of Innovation and Fusion Research, Troitsk 142190, Russia*

(Received 27 February 2013; published 3 May 2013)

Air plasma density decay in a filament produced by an intense femtosecond laser pulse in an external electric field was investigated experimentally and theoretically. It was demonstrated by means of the terahertz scattering technique that the rate of plasma decay decreases with increasing electric field. At the electric field of 7 kV/cm the lifetime of plasma with the density above 10^{16} cm^{-3} was prolonged from 0.5 ns to 1 ns. Numerical simulation of electron density decay and electron temperature evolution was performed, taking into consideration dissociative and three-body electron-ion recombination as well as formation of complex positive ions. The simulation showed that under the electric field the electron temperature evolves nonmonotonically and passes through a minimum due to varying contribution of electron-ion collisions to electron heating in the field. The rate of three-body electron recombination with O_2^+ ions of $2 \times 10^{-19}(300/T_e)^{9/2}$ cm^6/s was found from the experimental measurements at electron temperatures in the 0.25–0.4 eV range and electron densities in the $10^{15}-10^{17}$ cm^{-3} range.

DOI: 10.1103/PhysRevE.87.053101 PACS number(s): 52.20.−j, 52.38.−r, 52.27.Cm, 52.50.Jm

I. INTRODUCTION

The filamentation of intense femtosecond laser radiation has been attracting intense interest since its first demonstration by Braun *et al*. in 1995 [1]. This effect is governed by the competition of two processes: self-focusing of a laser beam due to Kerr nonlinearity and defocusing from photoexcited plasma. A long plasma channel can be formed due to filamentation. The subsequent plasma density decay plays a key role for different possible filament applications, such as lightning protection [2], atmospheric remote sensing [3], microwave guiding [4], terahertz generation [5], etc. Different experimental methods were used to measure the dynamics of electron density during filament decay. On the subnanosecond time scale, interferometry [6,7], transverse [8–10], and longitudinal [11] diffractometry were used. Direct measurements by transverse interferometry realized in [7] showed that plasma density in a single filament reaches 10^{17} cm^{-3} and decays by a factor of 5 within 300 ps. In [7], the terahertz scattering technique was also proposed to measure electron density in the filament. Measurements with this method demonstrated that plasma density decreased by 2 orders of magnitude (to 10^{15} cm^{-3}) for 2 ns after the filament initiation, in agreement with the qualitative results obtained by the diffractive method [8,10,12]. Over longer time intervals (tens of nanoseconds), plasma conductivity measurements were used [8,13–17]. Following this approach, the authors obtained plasma density by measuring the electric current flowing through the plasma located in a longitudinal external electric field [13] or using the potential drop caused by plasma screening in a transverse external electric field [17].

Theoretical investigation of filament plasma decay is generally based on simplified models (see, for instance, [8,14,16,18–20]). These models consider one species of positive ions and one species of negative ions. It is assumed that the loss of electrons is governed by two-body dissociative, electron-ion recombination and, at longer times (several nanoseconds), by electron attachment to O_2 molecules; the recombination and attachment rates are usually assumed to be constant and their magnitudes are adjusted to obtain agreement between calculations and measurements. In reality, electron loss rates depend on electron temperature that decays on the same time scale as the electron density in the filament plasma [12]. Therefore, consistent simulation of filament plasma decay should be based on simultaneous calculation of electron density and temperature decay. This has been done in Ref. [12] assuming (i) that electron temperature relaxation is governed by electron-impact excitation and electron elastic collisions with molecules and (ii) that the energy of all electrons is approximately equal to the electron temperature. These approximations are rather crude and can be used only to estimate electron temperature. Recently a much more consistent approach has been developed in Ref. [7]. In that work, the electron energy distribution in the filament plasma was assumed to be Maxwellian, whereas the electron temperature evolution was simulated taking into account different inelastic electron-molecule interactions, including electron-impact excitation of rotational, vibrational, and electronic levels of molecules. These interactions are generally used to calculate electron rate and transport properties in weakly ionized gases and plasma subjected to external electric fields [21–24].

Fast plasma decay observed in the experiments imposes significant limits for filament applications such as lightning protection, atmospheric remote sensing, and so on. Several approaches were proposed to increase plasma lifetime. It was shown that on the tens of nanoseconds time scale, plasma lifetime may be prolonged using an additional high-power nanosecond laser [25,26] or a sequence of femtosecond laser pulses [14,27]. In a recent paper [28], a sequence of seventeen 60-fs pulses with 15-ns separation between them and 60-mJ total energy was used. It was shown by measuring the plasma conductivity and fluorescence that the pulses with

*bosbor@ufp.appl.sci-nnov.ru

such parameters lead to an increase in the filament lifetime up to the microsecond range. In Ref. [16], it was shown that a Bessel-like nanosecond laser pulse of high energy (250 mJ) can restore the plasma at delays as large as several milliseconds (after the passage of a femtosecond laser pulse) due to electron detachment from negative ions followed by electron multiplication in an avalanche process. Another way to slow down plasma decay is to apply an external electric field along the filament. In Ref. [14] it was demonstrated that application of high voltage between two pointlike electrodes placed near the plasma filament resulted in prolongation of the plasma lifetime from 20 to 60 ns for an electric field of 3.5 kV/cm. It is important, however, that all these results were obtained on long time scales when the plasma density was rather small, below 10^{15} cm^{-3}, and have limited interest for the above-mentioned practical applications.

The goal of this paper is to investigate experimentally and theoretically a decrease in the rate of plasma density decay in a filament with applied external electric field on a subnanosecond time scale when plasma density is high (10^{15}–10^{17} cm^{-3}). For measuring plasma density we used the terahertz scattering technique [7]. The theoretical investigation is based on the approach developed in Ref. [7], which was extended to take into consideration external electric field. We considered electron heating in an external electric field that influences the rates of electron-ion recombination. Comparison between numerical simulation and experimental results allowed finding the rate of three-body electron recombination with O_2^+, the process that is poorly known for molecular ions.

The paper is organized as follows. The experimental setup, measurement technique, and experimental results are presented in Sec. II. Section III contains the theoretical model and its comparison with experiment. Section IV summarizes our results. The method for terahertz scattering calculation is presented in the Appendix.

II. PLASMA DENSITY MEASUREMENT: SETUP AND METHOD

A plasma filament was excited by a multi-millijoule Ti:sapphire laser system generating 60-fs pulses with 795-nm central wavelength and 10-Hz repetition rate. In the experimental setup (Fig. 1), the laser pulse was split into two parts. The first (pump) pulse with the energy of ~4 mJ was focused in air at ambient pressure by a spherical mirror with 125-cm focal length and produced a filament ~7 cm long near the mirror focus. Two circular plane electrodes (25 cm in diameter) with pinholes (2 mm in diameter) in the center for transmission of laser radiation were placed coaxially with the filament at a distance of 5 cm. Thus the filament fully overlapped the gap between the electrodes. High voltage was applied between the electrodes to induce external electric field E in the region of the plasma filament. Due to air discharge stimulated by the filament [29], the maximum electric field was limited to 7–8 kV/cm.

For investigation of plasma density decay in the external electric field we measured the scattering of the probe terahertz pulses. These pulses were generated in a 2-mm-thick ZnTe crystal by the laser pulses passed through a delay line. The terahertz pulses had a duration of ~1 ps with the spectrum

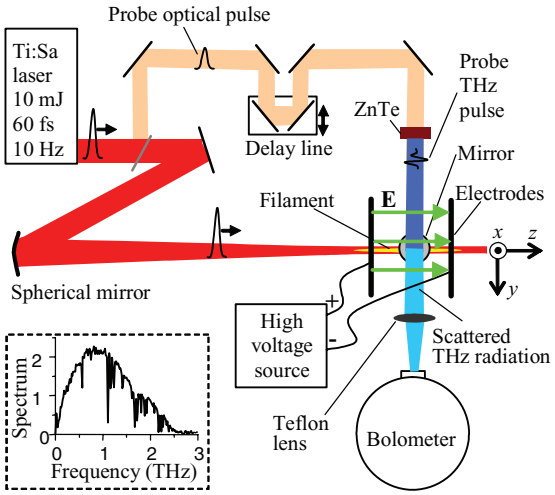

FIG. 1. (Color online) Experimental scheme for measuring plasma decay in a filament.

centered near 0.9 THz (see the inset in Fig. 1). These pulses were directed to the filament transversely to the laser path along the x axis (in the direction normal to the picture plane in Fig. 1). Part of the terahertz radiation scattered normally along the y axis was collected into the input of a liquid-He-cooled InSb hot-electron bolometer (QMS Instruments) by a Teflon lens ($D = 50$ mm, $F = 70$ mm) placed at ~20 cm from the filament. Efficient terahertz scattering was achieved because the transverse size (~150 μm) of the plasma channel was comparable with the terahertz wavelength and the plasma density was close to the critical value corresponding to the terahertz frequency.

During the experiment, we found that the laser pulse filamentation in the external electric field was accompanied by generation of a terahertz radiation comparable to the scattered probe terahertz radiation. We observed an approximately square-law dependence of the terahertz radiation energy generated in the filament on the applied electric field E [Fig. 2(a)], in agreement with the earlier publications [30,31].

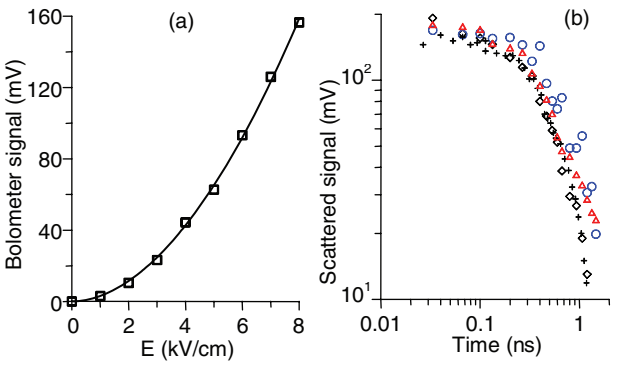

FIG. 2. (Color online) (a) Bolometer signal as a function of the external electric field E in the absence of probe terahertz pulses (boxes). The curve fits the data by the function $\sim E^n$ with $n = 1.9$. (b) Scattered signal as a function of the time delay of probe terahertz pulse for $E = 0$ kV/cm (diamonds), $E = 3$ kV/cm (triangles), and $E = 7$ kV/cm (circles). Crosses show the scattered signal obtained in Ref. [7] and normalized to the present data.

The terahertz radiation generated in the filament and probe terahertz radiation were detected by the bolometer simultaneously. The difference between the two signals measured with the probe terahertz pulse and without it gave the required scattered signal. Figure 2(b) shows the scattered signal as a function of the time delay for different values of applied electric field E. Our previous results obtained for $E = 0$ in Ref. [7], after the renormalization (crosses) agrees well with the present data (diamonds). During the first 200–400 ps (depending on the applied electric field E) of plasma decay the scattering signal does not significantly change and after that it decreases by more than an order of magnitude in 1 ns. Application of an external electric field leads to slowing down the terahertz scattered signal decay. Large signal fluctuations were obtained at $E = 7$ kV/cm, because in this case the energy of the scattered probe terahertz pulse was comparable to (or even less than) the energy of the terahertz radiation generated in the filament.

Evaluation of the plasma density from the scattered terahertz signal was based on the numerical code calculating scattering coefficient η of the pulsed electromagnetic radiation from the plasma channel (see Appendix). The code accounts for radially symmetric plasma density distribution $n_e(r)$, electron collisions in the plasma ν, and the terahertz spectrum taken from the experiment (see the inset in Fig. 1). To bring into accord the experimental scattered terahertz signal data with the calculated scattering coefficient η we used calibration on the basis of the previous optical interferometry measurements (Ref. [7]). The plasma density distribution $n_e(r) = n_{e0}\exp[-(r/r_0)^{12}]$ with $r_0 = 65\ \mu$m and $n_{e0} = 2.5 \times 10^{16}$ cm^{-3} at a time delay of 300 ps acquired from the interferometeric data was set as a reference point for $E = 0$. For this point the reference scattering coefficient was calculated with the code and was matched to the scattered signal measured by the bolometer. With this calibration taken into consideration, plasma density was obtained for other time delays and applied electric field by matching the calculated and experimental scattered signals. Note that in the calculations the shape of the density distribution was fixed and the electron collision frequency was taken into account as a function of the time delay. (The time evolution of electron temperature responsible for the collision frequency is discussed in Sec. III.)

The dynamics of the plasma density extracted from the experimental data is shown in Fig. 3 by symbols. We observed the fast decay of electron concentration about 10–20 times in ~1 ns. The rate of the plasma decay decreases in the presence of external electric field. For example, the plasma density for 1-ns time delay and $E = 7$ kV/cm is approximately twice as large as that for $E = 0$. For electric fields $E = 3$ and 7 kV/cm the difference is less pronounced.

Note that filament parameters (plasma density and diameter) may be estimated by the terahertz scattering technique without interferometric calibration, solely on the basis of the terahertz scattering data. Let us first discuss the calculated dependence of the scattering coefficient η on the plasma parameters. Figure 4 shows η as a function of plasma density n_{e0} for different plasma channel diameters and collision frequencies of electrons ν. The saturation of the scattering coefficient is observed at some threshold plasma density $n_{\rm th}$, which depends on the plasma channel diameter. For

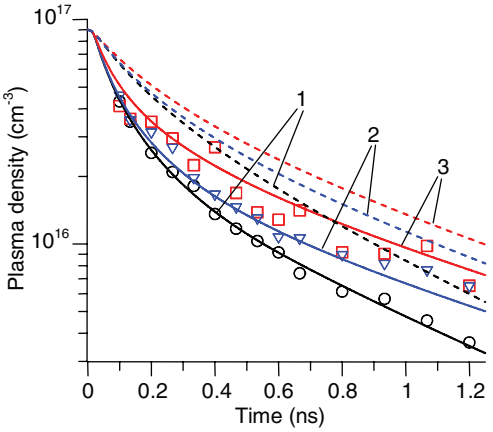

FIG. 3. (Color online) Time evolution of electron density during plasma decay at different values of the external electric field. The symbols are our measurements, the curves correspond to the calculations using the three-body electron recombination rate (dashed curves) calculated in [41] or (solid lines) adjusted in this work to reach agreement with the measurements. $E = 0$ (curves 1), 3 kV/cm (curves 2), or 7 kV/cm (curves 3).

large diameters (>300 μm), $n_{\rm th}$ is very close to a critical concentration $n_{\rm cr}$ for the central frequency of the terahertz pulse ($n_{\rm cr} = 10^{16}$ cm^{-3} for 0.9-THz central frequency). The agreement between $n_{\rm th}$ and $n_{\rm cr}$ is rather good for a 130-μm plasma channel diameter (curves 2, 3, and 4). For smaller diameters $n_{\rm th}$ shifts to a higher plasma concentration and the tendency of η to saturation becomes more gradual (curve 5). This is explained by the fact that for such a small channel diameter (<100 μm) the skin effect starts to play a significant role. The saturation values of the scattering coefficient from the filament agree well with the scattering coefficients from the metal wire with the corresponding radius (curves 1′, 2′, and 5′). For $n_{e0} \ll n_{\rm th}$, the scattering coefficient

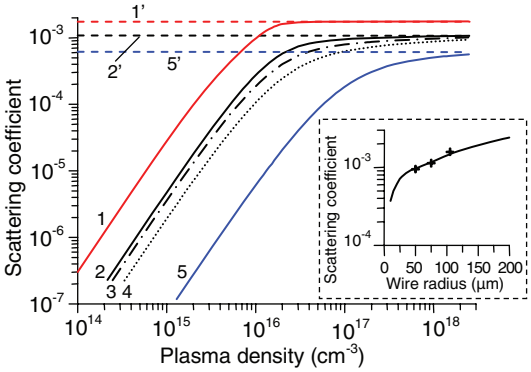

FIG. 4. (Color online) Terahertz scattering coefficient η of plasma cylinder with plasma density distribution $n_e = n_{e0}\exp[-(r/r_0)^{12}]$ and $r_0 = 150\ \mu$m (curve 1), 65 μm (curve 2), and 20 μm (curve 5) as a function of n_{e0} for collisionless plasma ($\nu = 0$) and plasma with $\nu = 2 \times 10^{12}$ s^{-1} (curve 3) and $\nu = 5 \times 10^{12}$ s^{-1} (curve 4) for $r_0 = 65\ \mu$m. The dashed curves show scattering coefficient of the metal wire with radius $r_m = 150\ \mu$m (curve 1′), 65 μm (curve 2′), and 20 μm (curve 5′). Inset: scattering coefficient of metal wire as a function of r_m (solid line). Crosses correspond to the normalized experimental data.

η scales as n_{e0}^2, which agrees with the analytical theory in Ref. [32] for the case of radiation scattering on a cylinder with dielectric properties close to unity. Electron collisions in plasma lead to a decrease in the scattering coefficient. But this effect is noticeable only if collision frequency ν significantly exceeds the central frequency of the probe terahertz pulse. For example, the scattering coefficients for $\nu = 2 \times 10^{12}$ s^{-1} and $\nu = 5 \times 10^{12}$ s^{-1} are, respectively, 20–30% and 2.5 times smaller than those in the collisionless case (see curves 3, 4, and 2 in Fig. 4, respectively).

The saturation of the scattering coefficient shown in Fig. 4 limits the range of the plasma density that can be measured by the terahertz scattering below $n_{\rm th}$. For our experimental parameters (plasma diameter near 130 μm) theoretical calculation gives $n_{\rm th} \sim 2 \times 10^{16}$ cm^{-3}. This value agrees well with experimental results. Indeed, according to the interferometric measurements of Ref. [7], at initiation of the filament the plasma density is $\sim 10^{17}$ cm^{-3} and then decreases to 2.5×10^{16} cm^{-3} at 300 ps. Thus the scattering signal should saturate in the first ~200–300 ps and then decrease in accordance with the experimental data shown in Fig. 2(b).

The terahertz scattering measurements may be calibrated using a metal wire. We placed the wire with known radius r_m instead of the filament and measured the scattered signal. The inset in Fig. 4 shows normalized experimental data for different r_m. The theoretical curve agrees well with the experimental results. Taking into account that the saturated scattered signal by the filament equals the scattered signal from the wire with corresponding radius, it is possible to calculate the radius of the filament. From this comparison we estimated the filament radius to be ~75–80 μm. This value is only slightly higher than that derived from the interferometric measurement (~65 μm). With known values of filament diameter and saturated scattered signal from the filament, the plasma density can be calculated for different time delays and applied electric field.

III. KINETIC MODEL, CALCULATED RESULTS AND DISCUSSION

To simulate loss of charged particles during plasma decay, we solved numerically a system of balance equations for electrons and positive ions:

$$\frac{dn_e}{dt} = -k_3(T_e) n_e^2 n_{p0} - n_e \sum_j k_{2j}(T_e) n_{pj} \qquad (1)$$

and

$$\frac{dn_{pj}}{dt} = Q_j - R_j. \qquad (2)$$

Here, n_{p0} is the density of O_2^+ ions, n_{pj} is the density of positive ions of the jth species, k_3 is the rate constant for three-body recombination of O_2^+ ions

$$e + O_2^+ + e \rightarrow O_2 + e, \qquad (3)$$

k_{2j} is the rate constant for two-body dissociative recombination of ions of the jth species, and Q_j and R_j are, respectively, the terms describing formation and loss of these ions. It was assumed that the plasma was uniform and the simulation was zero dimensional. The loss of charged particles due to ambipolar diffusion was neglected; this effect could be important under the conditions studied only for $t > 10^{-5}$ s, the time that is several orders of magnitude longer than the characteristic time of plasma decay in our experiment. The characteristic time of electron attachment to oxygen molecules in atmospheric pressure air is around 10 ns (see the attachment coefficient in [23]), much longer than the time of plasma decay in our case; therefore electron attachment was also neglected.

TABLE I. Reactions and rates of electron-ion recombination and ion conversion.

No.	Reaction	Rate coefficient
1	$e^- + O_2^+ \rightarrow O + O$	$1.95 \times 10^{-7}(\frac{300}{T_e})^{0.7}$ cm^3/s [a]
2	$e^- + O_2^+ + e^- \rightarrow O_2 + e^-$	See text
3	$e^- + O_2^+N_2 \rightarrow N_2 + O_2$	$1.3 \times 10^{-6}(\frac{300}{T_e})^{1/2}$ cm^3/s [b]
4	$e^- + O_4^+ \rightarrow O_2 + O_2$	$4.2 \times 10^{-6}(\frac{300}{T_e})^{1/2}$ cm^3/s [c]
5	$e^- + O_2^+H_2O \rightarrow O_2 + H_2O$	$2 \times 10^{-6}(\frac{300}{T_e})^{1/2}$ cm^3/s [d]
6	$O_2^+ + 2N_2 \rightarrow O_2^+N_2 + O_2$	$0.9 \times 10^{-30}(\frac{300}{T})^2$ cm^6/s [b]
7	$O_2^+N_2 + N_2 \rightarrow 2N_2 + O_2^+$	$1.1 \times 10^{-6}(\frac{300}{T})^{5.3} \times \exp(\frac{-2357}{T})$cm^3/s [b]
8	$O_2^+ + 2O_2 \rightarrow O_4^+ + O_2$	$2.4 \times 10^{-30}(\frac{300}{T})^{3.2}$ cm^6/s [b]
9	$O_4^+ + O_2 \rightarrow O_2^+ + 2O_2$	$3.3 \times 10^{-6}(\frac{300}{T})^4 \times \exp(\frac{-5030}{T})$cm^3/s [b]
10	$O_2^+N_2 + O_2 \rightarrow O_4^+ + N_2$	10^{-9}cm^3/s [b]
11	$H_2O + O_2^+ + M \rightarrow O_2^+H_2O + M$ M = O_2, N_2	2.8×10^{-28}cm^6/s [d]

[a]References [33,34].
[b]Reference [23].
[c]Reference [34].
[d]Reference [35].

Table I shows reactions taken into account in the simulation and their rate coefficients. In our case, the loss of electrons is controlled by their recombination with positive molecular ions. The rate of electron-ion recombination strongly depends on the positive ion composition, which changes with time during plasma decay. Under the action of the femtosecond laser pulse, only O_2^+ ions with relatively low (12 eV) ionization energy are produced in air. Complex ions (O_4^+ and $O_2^+N_2$) can be formed due to ion-molecule reactions only during plasma decay prior to recombination with electrons. In ambient air, the mole fraction of H_2O molecules can be around 1%. Therefore we took into account the formation of $O_2^+H_2O$ ions and their recombination with electrons for air with 1% H_2O.

Under the conditions of our experiment, the time of electron energy relaxation is comparable with the lifetime of the plasma. Therefore when simulating plasma decay it was necessary to study simultaneously electron temperature relaxation and the evolution of electron and ion densities. We assumed that the electron energy distribution is Maxwellian. This assumption is satisfied in our case because the frequency of the electron-electron collisions ν_{ee} is much higher than the frequency of electron energy exchange in collisions with molecules ν_ε. For instance, we have $\nu_\varepsilon \sim 10^9$ s^{-1} and $\nu_{ee} \sim 10^{13}$ s^{-1} in atmospheric pressure air for an average electron energy of 0.1 eV and $n_e = 10^{16}$ cm^{-3}. Electron temperature T_e

was obtained from a numerical solution of the electron energy conservation equation [35]:

$$\frac{3}{2}\frac{dT_e}{dt} = e\,w\,E - \frac{3}{2}(T_e - T)\,\nu_\varepsilon(T_e) + I\,k_3\,n_e n_p - T_e^2\frac{dk_3}{dT_e}n_e n_p - T_e^2\sum_j \frac{dk_{2j}}{dT_e}n_{pj}, \quad (4)$$

where w is the electron drift velocity, T is the gas temperature, $\nu_\varepsilon(T_e)$ is the frequency of electron energy relaxation in collisions with molecules, and I is the ionization energy of O_2 molecules. The first term on the right-hand side of Eq. (4) corresponds to electron heating in an external electric field. The last three terms on the right-hand side of Eq. (4) describe the effect of the so-called "recombination heating," which is important when the loss of electrons is dominated by electron-ion recombination. The third term proportional to I is due to the fact that the energy released in the reaction (3) is spent on the heating of free electrons, neglecting radiation emission and molecule dissociation. The presence of the fourth and fifth terms on the right-hand of Eq. (4) is explained by the fact that the probability of recombination increases with decreasing electron energy. As a result, the predominant loss of low-energy electrons leads to an increase in electron temperature.

The frequency of electron energy relaxation ν_ε was calculated by analogy with [36]. The initial value of T_e was assumed to be equal to the ionization energy of O_2. The calculated results are almost independent of this magnitude because the rate of electron energy exchange decreases with decreasing energy. Indeed, high-energy electrons rapidly lose their energy in the inelastic collisions with excitation of electronic states of N_2 molecules and with dissociation of O_2 molecules [24,37]; however, when the electron energy decreases below the energy thresholds of these processes, the frequency ν_ε drops drastically. The reason is that such electrons lose their energy only in elastic collisions and in the inelastic collisions with vibrational and rotational excitation of molecules.

To simulate the temporal evolution of T_e during the plasma decay in an external electric field, the electron drift velocity w is required. In a weakly ionized plasma, the electron energy distribution and electron transport and rate properties are controlled by electron collisions with neutral particles and the magnitude of w depends on the reduced electric field E/N, where N is the gas number density [24,37]. At sufficiently high electron densities, electron-electron and electron-ion collisions are also important. In this case, the magnitude of w depends on the ionization degree, $\alpha = n_e/(N + n_e)$, too. We calculated the electron drift velocity using the computer code [38]. This code solves the Boltzmann equation for electrons taking into account electron energy losses due to electronic, vibrational, and rotational excitation of N_2 and O_2, dissociation and ionization of these molecules, electron attachment to O_2, and elastic scattering of electrons by molecules and charged particles. Figure 5 shows the calculated results for $E/N =$ 12.2 and 28.6 Td (1 Td $= 10^{-17}$ V cm^2) as a function of the electron density for atmospheric pressure air. These values of E/N correspond to $E = 3$ and 7 kV/cm, respectively, at atmospheric pressure and room temperature. The calculations

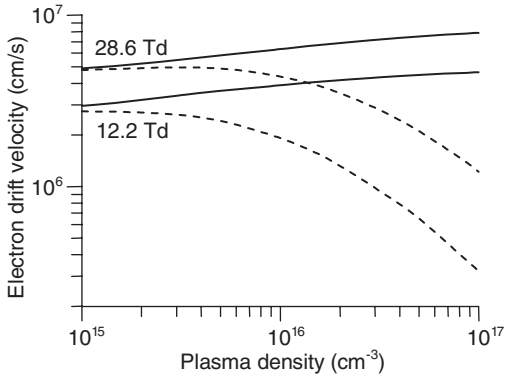

FIG. 5. Electron drift velocity in atmospheric pressure air for various reduced electric fields (1 Td $= 10^{-17}$ V cm^2) as a function of electron density. Calculations were carried out taking into account (dashed curves) and neglecting (solid curves) electron-ion collisions.

were carried out for two cases: (i) neglecting electron-ion collisions and (ii) with allowance for electron-ion collisions. In the absence of electron-ion interaction, the magnitude of w increases with increasing n_e due to electron-electron collisions affecting the electron energy distribution. The situation changes when considering electron-ion collisions. Here, the electron drift velocity decreases with increasing electron density. This effect is negligible at $n_e < 10^{15}$ cm^{-3}. The impact of electron-ion collisions leads to a decrease in w approximately (i) by an order of magnitude at $n_e = 10^{17}$ cm^{-3} and (ii) by one half at $n_e = 10^{16}$ cm^{-3}. Under the conditions studied, the electron density varied from 10^{17} to 10^{15} cm^{-3}, and it was necessary to take into account the influence of electron-ion collisions. It is worth noting that there are a number of numerical codes to solve the electron Boltzmann equation (see, for instance, Boltsig + [39]) that consider electron-electron collisions and neglect electron-ion interactions. Using these codes, a serious error could be obtained when simulating the plasma decay in an external electric field at sufficiently high plasma densities.

The rates of ion charge exchange, ion conversion and two-body dissociative recombination for O_2^+ and O_4^+ ions given in Table I were taken from measurements (see the references therein). Information about the rates of dissociative recombination for $O_2^+N_2$ and $O_2^+H_2O$ ions is absent, and we used estimated magnitudes suggested previously for these rates in Refs. [23,35], respectively. The rate for three-body electron-ion recombination has been measured (see Ref. [40]) only at electron densities that are several orders of magnitudes lower than those obtained in our case. This reaction is a multistep elementary process; therefore its rate constant depends on electron density. As a first approximation, we used the three-body recombination rate calculated in [41] for H^+ ions in the electron density range studied in this work. The magnitude of this rate is almost independent of atomic ion species at $T_e < 3000$ K [40].

Figure 3 shows the calculated time evolution of electron density in a plasma filament during its decay using the three-body recombination rate calculated in [41] (dashed lines). The evolution of T_e was simultaneously simulated using Eq. (4). The calculated rate of plasma decay was much lower than

that measured in the experiment. The difference between the calculated and measured values of n_e reached a factor of 2. The calculations showed that complex ions have no time to be formed at $t < 0.5$ ns and consequently, it was not possible to reach agreement between the calculations and measurements by varying the rates of dissociative recombination with these ions. The rate of two-body dissociative recombination with O_2^+ ions has been measured in many studies [34] and the discrepancy between available data is small. Therefore the main cause of the disagreement between the calculations and measurements seems to be associated with the rate of three-body recombination for O_2^+ ions.

Three-body recombination of electrons with molecular ions, the third body being an electron, has been studied experimentally only for He_2^+ ions [42], whereas no theoretical studies of this process for real molecular ions have been carried out. The measured rate of three-body recombination for He_2^+ ions turned out to be much lower than that for atomic ions. However, it seems that recombination of He_2^+ ions differs seriously from that for other molecular ions. This is well understood for dissociative recombination of molecular ions [34] and could also be expected for three-body recombination. At the same time, the authors of Ref. [43] hypothesized that the rate of three-body recombination for molecular ions can be an order of magnitude higher than that of three-body recombination for atomic ions due to the channel

$$e + A_2^+ + e \rightarrow A + A + e. \quad (5)$$

According to the calculation made in Ref. [43], the T_e dependence of the recombination rate for molecular ions could be weaker than that of the recombination rate for atomic ions. The difference between three-body recombination of molecular and atomic ions is associated with the mechanism of this process that proceeds in many stages [40,43]. In the first stage, a free electron is captured by an ion in a three-body collision to form a neutral particle in a highly excited Rydberg state. Then the weakly bonded electron loses its energy diffusively due to collisions with free electrons and due to radiation transitions. The process is finished when the electron descends to a sufficiently low energy level of the neutral particle. It was shown in [43] that, in the case of molecular ions, the quenching rate for highly excited states of neutral particles could be drastically increased due to dissociation of highly excited molecular states.

In Ref. [43], a hypothetical model molecular system was studied in which the energy spectrum of highly excited states was assumed to be similar to that of a hydrogen atom. The only exception was one effective highly excited state that could quickly decay due to molecule predissociation. Recently the effect studied in [43] has been considered for recombination of real molecular ions when the third body is a neutral particle [44]. In particular, this mechanism of three-body recombination was used to explain the difference between the available measurements of the recombination rates for H_3^+ ions in plasma afterglow with sufficiently high particle densities and storage ring data obtained at low densities. In addition, the hypothesis that the rate of three-body electron recombination with O_2^+ ions is much higher than that of three-body electron recombination with atomic ions was used to explain time-resolved measurements of electron density during air plasma decay after a high-voltage nanosecond discharge [45].

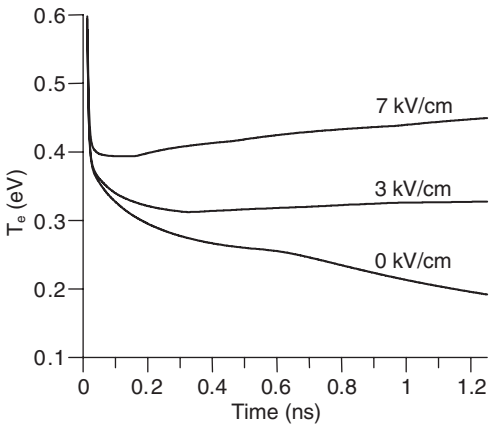

FIG. 6. Time evolution of electron temperature. The curves correspond to the same conditions as those in Fig. 3.

Assuming that the rate of three-body recombination for molecular ions can be much higher than the corresponding quantity for atomic ions, we varied the magnitude of the rate of three-body recombination for O_2^+ ions k_3, supposing that $k_3 = A\,(T_e/300\ \mathrm{K})^{-n}$ with $n = 4.5$, the typical T_e dependence for the rate of this process [40]. In this case, we conjectured that the recombination proceeds via the channel (5) and that the energy released in this process is spent on dissociation and excitation of O atoms instead of the heating of free electrons. Therefore, in this calculation, we neglected the third term on the right-hand side of Eq. (4). The agreement between the calculated and measured values of n_e was obtained for $A = 2 \times 10^{-19}$ cm^6 s^{-1} (see Fig. 3, solid lines). In this case, the rate for three-body recombination of O_2^+ ions is higher than the rate for H^+ ions calculated in [41] for the same range of electron densities by a factor of 4.8 at $T_e = 2000$ K and by a factor of 9.2 at $T_e = 4000$ K. It should be noted that agreement could also be obtained for other values of A when varying the value of n. For instance, the calculated electron density fits well the measurements at $A = 10^{-19}$ cm^6 s^{-1} and $n = 4.2$.

Figure 6 shows the calculated time evolution of the electron temperature when good agreement between the simulation and our measurements was obtained. Here, the electron temperature decreased with time during the plasma decay in the absence of electric field, whereas in a nonzero electric field the electron temperature, after a sharp drop, passed through a minimum and tended to a constant value due to electron heating in a given electric field at low ionization degrees. The obtained minimum is associated with electron-ion collisions leading to an increase in the electron drift velocity with decreasing electron density. As a result, a decrease in n_e during the plasma decay caused an increase in the energy gained by the electrons in an electric field as long as the electron drift velocity depended on n_e.

Figure 7 shows the time evolution of the ion composition during the plasma decay in the absence of electric field and in electric field of 7 kV cm^{-1}. Under the conditions studied the positive ion composition is dominated by O_2^+ ions.

The time evolution of the frequencies of electron loss through various recombination channels is presented in

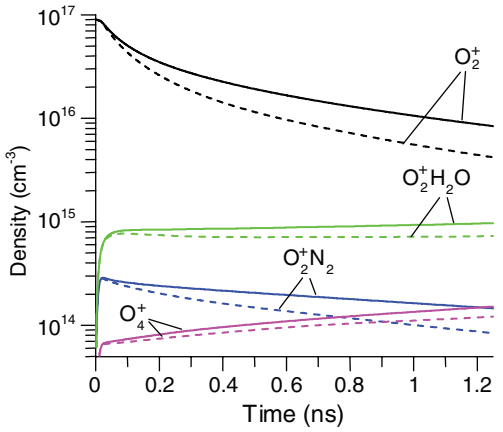

FIG. 7. (Color online) Time evolution of ion densities during plasma decay at $E = 0$ (dashed curves) and at $E = 7$ kV/cm (solid curves).

Fig. 8. Three-body electron-ion recombination is the dominant mechanism of plasma decay at $t < 0.7$ ns in the absence of electric field. The time interval in which this process is important becomes shorter when the plasma decays in the electric field because of additional electron heating. At longer times dissociative electron recombination with complex ions becomes more important. The rates for these reactions are poorly known and the calculated results are not reliable in this case. The rates for dissociative recombination of O_2^+ ions are understood much better, within an accuracy of around 20%. This allows, using the measured data on the time-resolved electron density, extraction of the values of the rate of three-body electron recombination with O_2^+ ions at various electron temperatures. In particular, the obtained values can be approximated by $k_3 = A(T_e/300\ \mathrm{K})^{-n}$ with $n = 4.5$ and $A = 2 \times 10^{-19}$ cm^6 s^{-1}. These values correspond to electron temperatures in the 0.25–0.4 eV range and to electron densities in the 10^{15}–10^{17} cm^{-3} range.

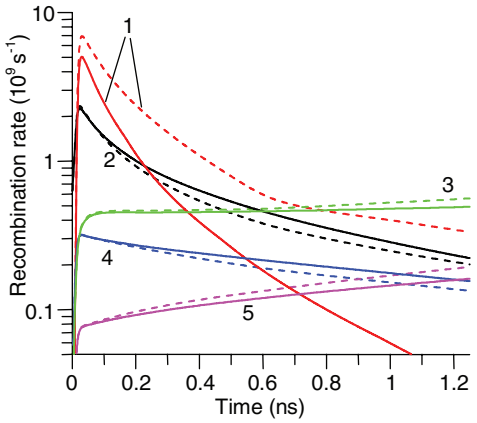

FIG. 8. (Color online) Time evolution of frequencies for three-body recombination of O_2^+ (curve 1) and two-body dissociative recombination for O_2^+ (curve 2), $O_2^+H_2O$ (curve 3), $O_2^+N_2$ (curve 4), and O_4^+ (curve 5). Calculations were carried out at $E = 0$ (dashed curves) and at $E = 7$ kV/cm (solid curves).

IV. CONCLUSIONS

The influence of external electric field on air plasma density decay in a femtosecond-laser-produced filament was studied by means of the terahertz scattering technique on the subnanosecond time scale. It was demonstrated that from the initial value of 10^{17} cm^{-3} plasma density decreases 10–20 times within ~1 ns, depending on the applied electric field. The increase of the electric field results in a slowing down of the plasma decay rate. At the maximum electric field of 7 kV/cm (limited by air discharge stimulated by the filament), the lifetime of a plasma with density above 10^{16} cm^{-3} was prolonged from 0.5 to 1 ns. The electron density and temperature evolution during the plasma decay was simulated simultaneously using the available rates of electron-ion recombination and electron-molecule interactions. The effect of three-body electron recombination with O_2^+ ions, the impact of formation and recombination of complex ions on electron density history, and the influence of recombination heating on electron temperature history were shown to be important during the decay of light filaments. It was necessary to consider these effects to obtain agreement between measurements and calculations under the studied conditions. The experimental data were used to obtain the rate of three-body electron recombination with O_2^+ ions for electron temperatures in the 0.25–0.4 eV range. This rate turned out to be much higher than the rate of the well-studied three-body electron recombination with atomic ions, in qualitative agreement with the hypothesis suggested in [43]. According to the calculations, during the plasma filament decay in an external electric field, the electron temperature decreases, passes through a minimum, and then increases to a stable value controlled by the electric field strength. This is explained by an increase in the electron drift velocity with decreasing density of charged particles due to electron-ion collisions that are important at high densities and become negligible at low ones.

ACKNOWLEDGMENTS

This work was supported in part by RFBR Grants No. 12-02-31598 and No. 12-02-33087, the Program of the Presidium of RAS, "Extreme Light Fields and Their Application" and Ministry of Education and Science of the Russian Federation through Agreement No. 11.G34.31.0011 and No. 14.B37.21.0770.

APPENDIX: TERAHERTZ SCATTERING CALCULATION

To simulate scattering of the terahertz pulse from the filament, the following model was used. An electromagnetic pulse propagates along the x axis and is incident perpendicularly on an infinitely long (along the z axis) plasma channel with a radially symmetric electron distribution $n_e(r)$ (see Fig. 1). The electromagnetic pulse is polarized along the z axis and has intensity spectral distribution $I(\omega)$ and Gaussian radial distribution $\sim \exp[-r^2/\ell^2(\omega)]$. The transverse size $\ell(\omega)$ is assumed to be much larger than the corresponding wavelength; therefore the approximation of a plane electromagnetic wave for each spectral component ω is used. In this approximation, the incident electric field in the Fourier domain E_z^i may be

written via a series expansion of the Bessel functions [32]

$$E_z^i(\omega,r,\varphi) = E_0(\omega)\sum_{l=-\infty}^{\infty}(-i)^l J_l(k_0 r)e^{il\varphi}, \qquad \text{(A1)}$$

where J_l is the Bessel function of the first kind, φ is the azimuthal angle in the y-x plane, $\varphi = 0$ corresponds to the direction of the x axis, $k_0 = \omega/c$, and c is the speed of light in vacuum. A Fourier component of the scattered field is written in a similar form:

$$E_z^s(\omega,r,\varphi) = \sum_{l=-\infty}^{\infty} a_l^s H_l^{(2)}(k_0 r)e^{il\varphi}, \qquad \text{(A2)}$$

where $H_l^{(2)}$ is the Henkel function of the second kind, and a_l^s are unknown coefficients. The smooth radial distribution of the plasma density $n_e(r)$ in the channel is approximated by a step function with finite steps M. In each mth step, the plasma density n_{em} is uniform in the region $r_m < r < r_{m+1}$, so the electric field is written as

$$E_z^m(\omega,r,\varphi) = \sum_{l=-\infty}^{\infty}\left[a_l^m J_l(k_m r) + c_l^m N_l(k_m r)\right]e^{il\varphi}, \qquad \text{(A3)}$$

where N_l is the Bessel function of the second kind, $k_m = \sqrt{\varepsilon_m}\omega/c$ is the wave number, $\varepsilon_m = 1 - \omega_{pm}^2/(\omega^2 - i\omega\nu)$ is the dielectric constant, ν is the electron collision frequency, $\omega_{pm} = \sqrt{4\pi n_{em}e^2/m}$, e and m are electron charge and mass, respectively. The magnetic field in vacuum and in the plasma channel can be written in a similar form. The coefficients a_l^s, a_l^m, and c_l^m are calculated by the code taking into account the boundary conditions.

The scattering coefficient is defined by $\eta = W_s/W_0$, where $W_0 = \pi\int_0^\infty d\omega I(\omega)\ell(\omega)^2$ is the incident energy of the terahertz pulse and W_s is the scattered terahertz energy over the range of angles from φ_1 to φ_2 in the x-y plane. The scattered terahertz energy is calculated by integration of the Pointing vector of the scattered radiation:

$$W_s = \frac{2}{\pi}\int_0^\infty d\omega\frac{c}{\omega}\ell(\omega)\int_{\varphi_1}^{\varphi_2} d\varphi|a_0^s + \sum_{l=1}^{\infty} 2\frac{a_l^s}{i^l}\cos(l\varphi)|^2. \qquad \text{(A4)}$$

In Eq. (A4), the transverse size $\ell(\omega)$ was calculated with allowance for diffraction of the terahertz beam with an initial FWHM size of 3 mm for all spectral components (this size corresponds to the FWHM optical spot of the probe beam divided by a factor of $\sqrt{2}$). The angles φ_1 and φ_2 were taken to be 80° and 100°, respectively, in accordance with conditions of the experiment.

[1] A. Braun, G. Korn, X. Liu, D. Du, J. Squier, and G. Mourou, Opt. Lett. **20**, 73 (1995).

[2] M. Rodriguez, R. Sauerbrey, H. Wille, L. Wöste, T. Fujii, Y.-B. André, A. Mysyrowicz, L. Klingbeil, K. Rethmeier, W. Kalkner, J. Kasparian, E. Salmon, J. Yu, and J.-P. Wolf, Opt. Lett. **27**, 772 (2002).

[3] J. Kasparian, M. Rodriguez, G. Méjean, J. Yu, E. Salmon, H. Wille, R. Bourayou, S. Frey, Y.-B. André, A. Mysyrowicz, R. Sauerbrey, J.-P. Wolf, and L. Wöste, Science **301**, 61 (2003).

[4] M. Châteauneuf, S. Payeur, J. Dubois, and J.-C. Kieffer, Appl. Phys. Lett. **92**, 091104 (2008).

[5] C. D. Amico, A. Houard, S. Akturk, Y. Liu, J. Le. Bloas, M. Franco, B. Prade, A. Couairon, V. T. Tikhonchuk, and A. Mysyrowicz, New J. Phys. **10**, 013015 (2008).

[6] Y.-H. Chen, S. Varma, T. M. Antonsen, and H. M. Milchberg, Phys. Rev. Lett. **105**, 215005 (2010).

[7] S. Bodrov, V. Bukin, M. Tsarev, A. Murzanev, S. Garnov, N. Aleksandrov, and A. Stepanov, Opt. Express **19**, 6829 (2011).

[8] S. Tzortzakis, B. Prade, M. Franco, and A. Mysyrowicz, Opt. Commun. **181**, 123 (2000).

[9] S. Tzortzakis, B. Prade, M. Franco, A. Mysyrowicz, S. Huller, and P. Mora, Phys. Rev. E **64**, 057401 (2001).

[10] G. Rodriguez, A. R. Valenzuela, B. Yellampalle, M. J. Schmitt, and K.-Y. Kim, J. Opt. Soc. Am. B **25**, 1988 (2008).

[11] F. Th'eberge, W. Liu, P. T. Simard, A. Becker, and S. L. Chin, Phys. Rev. E **74**, 036406 (2006).

[12] Z. Sun, J. Chen, and W. Rudolph, Phys. Rev. E **83**, 046408 (2011).

[13] S. Tzortzakis, M. A. Franco, Y.-B. André, A. Chiron, B. Lamouroux, B. S. Prade, and A. Mysyrowicz, Phys. Rev. E **60**, R3505 (1999).

[14] J. Zhu, Z. Ji, Y. Deng, J. Liu, R. Li, and Z. Xu, Opt. Express **14**, 4915 (2006).

[15] S. Eisenmann, A. Pukhov, and A. Zigler, Phys. Rev. Lett. **98**, 155002 (2007).

[16] B. Zhou, S. Akturk, B. Prade, Y.-B. Andre, A. Houard, Y. Liu, M. Franco, C. D'Amico, E. Salmon, Z.-Q. Hao, N. Lascoux, and A. Mysyrowicz, Opt. Express **17**, 11450 (2009).

[17] D. Abdollahpour, S. Suntsov, D. G. Papazoglou, and S. Tzortzakis, Opt. Express **19**, 16866 (2011).

[18] H. Yang, J. Zhang, Y. Li, J. Zhang, Y. Li, Z. Chen, H. Teng, Z. Wei, and Z. Sheng, Phys. Rev. E **66**, 016406 (2002).

[19] X. Chen, H.-B. Jiang, and Q.-H. Gong, Chin. Phys. Lett. **23**, 1482 (2006).

[20] N. Vujicic, H. Skenderovic, T. Ban, D. Aumiler, and G. Pichler, Appl. Phys. B **82**, 377 (2006).

[21] M. Capitelli, C. M. Ferreira, B. F. Gordiets, and A. I. Osipov, *Plasma Kinetics in Atmospheric Gases* (Springer, Berlin, 2000).

[22] Z. Lj. Petrovic, S. Dujko, D. Maric, G. Malovic, Z. Nikitovic, O. Sasic, J. Jovanovic, V. Stojanovic, and M. Radmilovic-Radenovic, J. Phys. D: Appl. Phys. **42**, 194002 (2009).

[23] I. A. Kossyi, A. Yu. Kostinsky, A. A. Matveyev, and V. P. Silakov, Plasma Sources Sci. Technol. **1**, 207 (1992).

[24] L. G. H. Huxley and R. W. Crompton, *The Diffusion and Drift of Electrons in Gases* (Wiley, New York, 1974).

[25] Z. Q. Hao, J. Zhang, Y. T. Li, X. Lu, X. H. Yuan, Z. Y. Zheng, Z. H. Wang, W. J. Ling, and Z. Y. Wei, Appl. Phys. B **80**, 627 (2005).

[26] G. Méjean, R. Ackermann, J. Kasparian, E. Salmon, J. Yu, and J.-P. Wolf, Appl. Phys. Lett. **88**, 021101 (2006).

[27] J. Zhonggang, Z. Jiabin, W. Zhanxin, G. Xiaochun, W. Wenyue, L. Jiansheng, and L. Ruxin, Plasma Sci. Technol. **12**, 295 (2010).
[28] X.-L. Liu, X. Lu, J.-L. Ma, L.-B. Feng, X.-l. Ge, Y. Zheng, Y.-T. Li, L.-M. Chen, Q.-L. Dong, W.-M. Wang, Z.-H. Wang, H. Teng, Z.-Y. Wei, and J. Zhang, Opt. Express **20**, 5968 (2012).
[29] N. L. Aleksandrov, E. M. Bazelian, N. A. Bogatov, A. M. Kiselev, and A. N. Stepanov, Plasma Phys. Rep. **34**, 1059 (2008).
[30] Y. Liu, A. Houard, B. Prade, A. Mysyrowicz, A. Diaw, and V. T. Tikhonchuk, Appl. Phys. Lett. **93**, 051108 (2008).
[31] A. Houard, Y. Liu, B. Prade, V. T. Tikhonchuk, and A. Mysyrowicz, Phys. Rev. Lett. **100**, 255006 (2008).
[32] J. R. Wait, *Electromagnetic Radiation from Cylindrical Structures* (Pergamon Press, New York, 1959).
[33] F. J. Mehr and M. A. Biondi, Phys. Rev. **181**, 264 (1969).
[34] A. I. Florescu-Mitchell and J. B. A. Mitchell, Phys. Rep. **430**, 277 (2006).
[35] N. L. Aleksandrov, S. V. Kindysheva, M. M. Nudnova, and A. Yu. Starikovskiy, J. Phys. D: Appl. Phys. **43**, 255201 (2010).
[36] N. L. Aleksandrov, S. V. Kindysheva, A. A. Kirpichnikov, I. N. Kosarev, S. M. Starikovskaia, and A. Yu. Starikovskii, J. Phys. D: Appl. Phys. **40**, 4493 (2007).
[37] Yu. P. Raizer, *Gas Discharge Physics* (Springer, Berlin, 1991).
[38] N. A. Dyatko, I. V. Kochetov, A. P. Napartovich, and A. G. Sukharev, http://www.lxcat.laplace.univ-tlse.fr/software/EEDF/.
[39] G. J. M. Hagelaar and L. C. Pitchford, Plasma Sources Sci. Technol. **14**, 722 (2005).
[40] L. M. Biberman, V. S. Vorob'ev, and I. T. Yakubov, *Kinetics of Non-Equilibrium Low-Temperature Plasmas* (Consultants Bureau, New York, 1987).
[41] D. R. Bates, A. E. Kingston, and R. W. P. McWhirter, Proc. R. Soc. A **267**, 297 (1962).
[42] M. A. Biondi, in *Principles of Laser Plasmas*, edited by G. Bekefi (Wiley, New York, 1976), Chap. 4.
[43] C. B. Collins, Phys. Rev. **140**, A1850 (1965).
[44] R. Johnsen and S. L. Guberman, Adv. At. Mol. Opt. Phys. **59**, 75 (2010).
[45] N. L. Aleksandrov, E. M. Anokhin, S. V. Kindysheva, A. A. Kirpichnikov, I. N. Kosarev, M. M. Nudnova, S. M. Starikovskaya, and A. Yu. Starikovskii, Plasma Phys. Rep. **38**, 179 (2012).